JACS
JOURNAL OF THE AMERICAN CHEMICAL SOCIETY
Article
pubs.acs.org/JACS

Copper Sulfide Nanocrystals with Tunable Composition by Reduction of Covellite Nanocrystals with Cu^+ Ions

Yi Xie,[†] Andreas Riedinger,[†] Mirko Prato,[†] Alberto Casu,[†] Alessandro Genovese,[†] Pablo Guardia,[†] Silvia Sottini,[‡] Claudio Sangregorio,[§] Karol Miszta,[†] Sandeep Ghosh,[†] Teresa Pellegrino,[†] and Liberato Manna*[,†]

[†]Department of Nanochemistry, Istituto Italiano di Tecnologia (IIT), via Morego, 30, 16163 Genova, Italy
[‡]Dipartimento di Chimica, Università di Firenze, Via della Lastruccia 3, Polo Scientifico, 50019 Sesto Fiorentino, Italy
[§]CNR-ISTM and INSTM, via Golgi 19, 20133 Milano, Italy

Supporting Information

ABSTRACT: Platelet-shaped copper sulfide nanocrystals (NCs) with tunable Cu stoichiometry were prepared from Cu-rich covellite ($Cu_{1.1}S$) nanoplates through their reaction with a Cu(I) complex ($[Cu(CH_3CN)_4]PF_6$) at room temperature. Starting from a common sample, by this approach it is possible to access a range of compositions in these NCs, varying from $Cu_{1.1}S$ up to Cu_2S, each characterized by a different optical response: from the metallic covellite, with a high density of free carriers and strong localized surface plasmon resonance (LSPR), up to Cu_2S NCs with no LSPR. In all these NCs the valency of Cu in the lattice stays always close to +1, while the average −1 valency of S in covellite gradually evolves to −2 with increasing Cu content; i.e., sulfur is progressively reduced. The addition of copper to the starting covellite NCs is similar to the intercalation of metal species in layered transition metal dichalcogenides (TMDCs); i.e., the chalcogen−chalcogen bonds holding the layers are progressively broken to make room for the intercalated metals, while their overall anion sublattice does not change much. However, differently from the TMDCs, the intercalation in covellite NCs is sustained by a change in the redox state of the anion framework. Furthermore, the amount of Cu incorporated in the NCs upon reaction is associated with the formation of an equimolar amount of Cu(II) species in solution. Therefore, the reaction scheme can be written as: $Cu_{1.1}S + 2\gamma Cu(I) \rightarrow Cu_{1.1+\gamma}S + \gamma Cu(II)$.

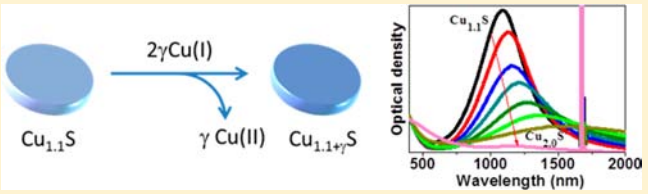

1. INTRODUCTION

$Cu_{2-x}S$ is a well-known p-type semiconductor exhibiting stoichiometry-dependent bandgap,[1] which makes nanocrystals (NCs) of this material appealing in diverse fields, like photovoltaics,[2,3] photocatalysis,[4] batteries,[5] chemical sensing,[6] and electronics.[7] Recent developments have been the elucidation of localized surface plasmon resonances (LSPRs) in $Cu_{2-x}S$ NCs. LSPRs, commonly observed in nanostructured metals like Au, Ag, and Cu nanoparticles,[8,9] have been now identified in various other nanomaterials, e.g., the binary copper chalcogenides ($Cu_{2-x}E$, E = S, Se, Te),[10−19] tin-doped indium oxide (ITO),[20−22] aluminum-doped zinc oxide (AZO),[23] the oxygen-deficient MoO_{3-x}[24] and WO_{3-x} NCs,[25] and also recently in Cu_3P[26] and GeTe NCs.[27] Zhao et al. first identified the near-infrared (NIR) absorption from $Cu_{2-x}S$ of various stoichiometries as a consequence of LSPR,[10] while Luther et al. systematically studied the NIR LSPR response of $Cu_{2-x}S$ NCs of different sizes and its dependence on the dielectric constant of the surrounding environment.[11] Other studies on the optical properties of $Cu_{2-x}S$, including CuS (covellite), in the NIR, have followed.[12,15]

To date, various synthetic approaches have yielded $Cu_{2-x}S$ NCs with controlled Cu stoichiometry.[15,28−33] $Cu_{2-x}S$ NCs with compositions equal to the limiting cases represented by CuS and Cu_2S (i.e., covellite and chalcocite, respectively) and also those with intermediate "x" values can be routinely made, although each one with a different synthetic procedure. This makes it difficult to compare their physical properties since each sample is also characterized by its own geometrical parameters and type of surface passivation. A notable exception is represented by $Cu_{2-x}S$ NCs with small values of x, i.e., with composition down to around $Cu_{1.9}S$, which were directly obtained by Luther et al. and Kriegel et al. starting from Cu_2S NCs upon their oxidation under air.[11,14] Procedures have been reported to tune the composition of copper sulfide powders from Cu_2S all the way to CuS, by means of reaction with iodine,[34] or to convert films of mixed Cu-chalcocite to chalcocite, roxbyite, and covellite, by sulfurization of metallic Cu films,[35] but it is unclear how such procedures can be extended to NCs while preserving their size, shape, and stability in solution.

We report here a simple approach to access several stoichiometries in colloidal copper sulfide NCs, starting from

Received: September 20, 2013
Published: October 15, 2013

   dx.doi.org/10.1021/ja409754v | J. Am. Chem. Soc. 2013, 135, 17630−17637

$Cu_{1.1}S$ NCs, up to Cu_2S. Our approach is based on the reaction of the as-synthesized covellite NCs with a Cu(I) complex, namely, tetrakis (acetonitrile) copper(I) hexafluorophosphate ($[Cu(CH_3CN)_4]PF_6$), a compound that is widely used in cation exchange reactions on NCs,[36−38] at room temperature. The advantage of this method lies in the fact that many NC samples of varying compositions can be prepared starting from a single batch of NCs, while preserving the original shape and overall size of the "parent" particles (apart from a maximum 6% increase in size due to incorporation of copper). It therefore provides us with a unique set of NCs on which we can study how structural and optical properties, as well as the valences of Cu and S in the NCs, evolve with variation of the Cu:S ratio.

We verified with the aid of several techniques that, as soon as the Cu stoichiometry in the NCs increased upon gradual addition of Cu(I) to the solution of the initial particles, the NCs underwent structural changes as well as evolution of their optical properties: the strong LSPR response of the initial covellite NCs red-shifted and decreased in intensity, until it disappeared for the NCs with Cu_2S composition. As proven by a combination of techniques (including X-Ray Photoelectron Spectroscopy and Electron Paramagnetic Resonance), the valency of Cu in all samples remained close to +1, throughout these chemical and structural transformations, while the initial average −1 valency of sulfur in covellite, due to the presence of S−Cu and S−S bonds in this structure, gradually evolved to −2 in samples with composition close to Cu_2S. This is consistent with a progressive decrease in the density of holes in the valence band, the latter having a strong contribution from the sulfur 3p orbitals in these compounds. We also verified via electron paramagnetic resonance spectroscopy that the increase in Cu stoichiometry in the NCs was matched by the formation of an equimolar amount of Cu(II) species in solution (see Scheme 1). While the detailed mechanisms of this overall reaction are at the present unclear, obviously the increase of Cu stoichiometry in the NCs, with progressive reduction in the valency of S even as that of Cu stays fixed, must occur at the expense of a fraction of the Cu(I) ions in solution, which are oxidized to Cu(II).

Scheme 1. $Cu_{1.1}S$ NCs with Covellite Phase Incorporating Additional Cu Species in Their Lattice upon Reaction with a Cu(I) Complex ($[Cu(CH_3CN)_4]PF_6$)[a]

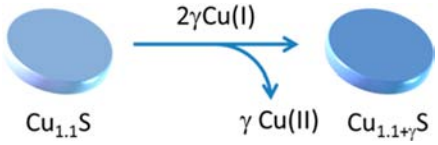

[a]The insertion is accompanied by the oxidation of an equimolar amount of Cu(I) species in solution to Cu(II).

2. EXPERIMENTAL SECTION

2.1. Materials. Tetrakis (acetonitrile) copper(I) hexafluorophosphate ($[Cu(CH_3CN)_4]PF_6$, 97%), copper (I) chloride (CuCl, anhydrous, 99.99%), tetrachloroethylene (TCE, spectrophotometric grade 99+%), oleylamine (OLAM, >70%), and octadecene (ODE, 90%) were purchased from Sigma-Aldrich; elemental sulfur (99+%) and trioctylphosphine (TOP) from Strem Chemicals; and isopropanol (anhydrous, 99.8%), ethanol (anhydrous, 99.9%), methanol (anhydrous, 99.9%), and toluene (anhydrous, 99.8%) from Carlo Erba reagents. All chemicals were used as received without further purification.

2.2. Heat-Up Synthesis of Covellite NCs. All procedures described here were carried out under air-free conditions. The "parent" covellite NCs were synthesized by a heat-up procedure. Using a standard Schlenk line, a sulfur solution was first prepared by degassing a mixture containing 0.032 g (1 mmol) of sulfur powder, 5 mL of OLAM, and 5 mL of ODE in a 50 mL three-neck flask, at 130 °C under vacuum for 30 min. The resulting clear yellow solution was then cooled to room temperature under nitrogen. An amount of 0.050 g (0.5 mmol) of CuCl was added to the sulfur solution, and the flask was pumped to vacuum at room temperature for 60 min, followed by heating to 200 °C under N_2 flow, with a ramp of 8 °C/min. Once at 200 °C, the reaction was run for an additional 30 min. The resulting dark green solution was cooled to room temperature and transferred to a nitrogen-filled glovebox, where it was washed three times with ethanol and redissolved in toluene. The NCs dissolved in toluene were carefully centrifuged at 1000 rpm for 2 min to remove the large nanoplates that were formed as a byproduct, which however represented a small fraction of the sample. Attempts were made to vary the shape of the NCs, departing from the reaction conditions described above. However, either we could still obtain covellite disks, although with broad size distributions, or the final sample was a mixture of phases.

2.3. Reaction of the As-Synthesized NCs with the Cu(I) Complex. All these reactions were performed at room temperature in a N_2-filled glovebox. A series of vials containing the NCs dissolved in toluene were prepared. In each vial, the total volume of solution was 5 mL, and the total amount of Cu was equal to 0.15 mmol (as determined by elemental analysis, see later). A stock solution of a Cu(I) complex (0.02 M) was prepared by dissolving 1.192 g of $[Cu(CH_3CN)_4]PF_6$ in 160 mL of anhydrous methanol. A different volume of this Cu(I) solution was then added to each vial of NC solution under magnetic stirring. Added volumes ranged from 2.25 mL (corresponding to 0.045 mmol of Cu(I)) to 45 mL (corresponding to 0.9 mmol of Cu(I)). Attempts to work with more concentrated solutions of Cu(I), to reduce the amount of added volume of Cu(I) solution, were not successful due to the low solubility of $[Cu(CH_3CN)_4]PF_6$ in methanol.

After the additions, the resulting samples were left stirring for 24 h. At this point, the NCs were separated from the solutions and purified by repeated dissolution in toluene and precipitation with acetonitrile. The number of purification steps varied depending on the type of analysis that had to be carried out: only one step, in the case of optical extinction measurements, to avoid aggregation effects that would red-shift and broaden the LSPR band; two steps for conventional TEM analysis; and three steps for all other measurements. In the case of EPR measurements (see Section 2.10) there was actually no need to perform such separation and purification of the NCs (see later); therefore, "crude" solutions were used.

2.4. Elemental Analysis. Inductively coupled plasma optical emission spectroscopy (ICP-OES), using a iCAP 6000 spectrometer (ThermoScientific), was used to quantify the Cu amount in the NCs, before and after their reaction with the Cu(I) complex (as described in Section 2.3), to estimate the amount of Cu incorporated in the NCs. The NCs were decomposed in the aqua regia (HCl/HNO_3 equal to 3:1 (v/v)) prior to measurements.

2.5. UV−vis−NIR Spectroscopy. Optical extinction spectra, both on solutions containing "as-synthesized" NCs and on those containing NCs after their reaction with the Cu(I) complex, were performed on a Varian Cary 5000 UV−vis−NIR absorption spectrophotometer in the 300−3200 nm wavelength range. Toluene or TCE was used as solvents for the measurements.

2.6. X-ray Diffraction (XRD). XRD patterns were recorded on a Rigaku SmartLab X-ray diffractometer. The X-ray source was operated at 40 kV and 150 mA. The diffractometer was equipped with a Cu source and a Göbel mirror (to obtain a parallel beam), and it was used in $2\theta/\omega$ scan geometry for the acquisition of the data. The specimens were prepared in a N_2-filled glovebox by drop casting the concentrated NC solution onto a zero background silicon substrate followed by drying. The PDXL software of Rigaku was used for phase identification.

dx.doi.org/10.1021/ja409754v | J. Am. Chem. Soc. 2013, 135, 17630−17637

2.7. Transmission Electron Microscopy (TEM). For conventional TEM observations, the samples were prepared by drop-casting concentrated NC solutions onto carbon-coated 200 mesh copper grids, and the measurements were performed with a JEOL JEM 1011 microscope operating at 100 kV accelerating voltage. High-resolution TEM (HRTEM), high angle annular dark field scanning TEM (HAADF-STEM), and energy-dispersive X-ray spectroscopy (EDS) analyses were performed with a JEOL JEM-2200FS microscope equipped with a field emission gun working at 200 kV, a CEOS spherical aberration corrector of the objective lens allowing for a spatial resolution of 0.9 Å, and an in-column Omega energy filter. The chemical composition of the NCs was determined by EDS, performed in STEM-HAADF mode, using a Bruker Quantax 400 system with a 60 mm^2 XFlash 6T silicon drift detector (SDD). For HRTEM analyses the NC solutions were drop-cast onto copper grids covered with an ultrathin amorphous carbon film, while for STEM-EDS analyses they were deposited onto carbon-coated aluminum grids and the measurements carried out using a holder with a beryllium cup.

2.8. X-ray Photoelectron Spectroscopy (XPS). The samples were prepared in the glovebox by drop-casting a few microliters of the NC solutions on a graphite substrate (HOPG, ZYB quality, NT-MDT) and then transferred to the XPS setup using an ad hoc transfer vessel to avoid air exposure. Measurements were performed on a Kratos Axis Ultra DLD spectrometer, using a monochromatic Al Kα source (15 kV, 20 mA). Wide scans were acquired at analyzer pass energy of 160 eV. High-resolution narrow scans were performed at constant pass energy of 10 eV and steps of 0.05 eV. The photoelectrons were detected at a takeoff angle of Φ = 0° with respect to the surface normal. The pressure in the analysis chamber was maintained below 7×10^{-9} Torr for data acquisition. The data were converted to VAMAS format and processed using CasaXPS software, version 2.3.15. The binding energy (BE) scale was internally referenced to the C 1s peak (BE for C−C = 285 eV).

2.9. Superconducting Quantum Interference Device (SQUID) Measurements. Samples were measured using a Quantum Design magnetometer. Magnetization curves were measured from −70 up to +70 kOe at 300 K. Samples were prepared in the glovebox by drop casting 500 μL of a NC solution on a Teflon tape and allowing the solvent to evaporate. After evaporation the sample was enwrapped and measured.

2.10. Electron Paramagnetic Resonance (EPR). Continuous-wave (CW) EPR spectra were recorded at 80 K with a Bruker Elexsys E500 spectrometer, equipped with a Super High Sensitivity Probehead and a continuous-flow[4] He cryostat (ESR900, Oxford Instruments). The measurements were performed at the X band (9.5 GHz), with a microwave power of 0.65 mW, and with a field modulation of 100 kHz and 7 G. The EPR tubes containing 300 μL of solution were filled and sealed in the glovebox and always placed at the same height in the resonant cavity. As the reference sample for the quantitation of Cu(II) species in the NC samples, we used solutions of $CuCl_2$ in methanol, with a concentration ranging from 0.25 to 4 mM. The area of the integrated EPR spectrum was directly related to the concentration of Cu(II) species via a linear fit as described in the Supporting Information (SI). The EPR spectra of the NCs were recorded on the crude solutions.

2.11. Fourier Transform Infrared (FTIR) Spectroscopy. FTIR spectra of NC thin films were recorded on a Vertex 70 V spectrophotometer. The details of the measurements are found in the SI.

RESULTS AND DISCUSSION

Figures 1 and 2 summarize the results of optical, structural, and morphological characterization of the "as-synthesized" NCs. These NCs had platelet shapes (see Figure 1C and Figure S1a of SI). Their crystal structure was covellite, as assessed by XRD (Figure 1B, bottom), HRTEM (Figure 2A), and selected area electron diffraction (SAED, see Figure S1b, SI) phase identification measurements. In situ elemental analysis via STEM-EDS yielded a Cu:S ratio of 1.1:1, close to that of the

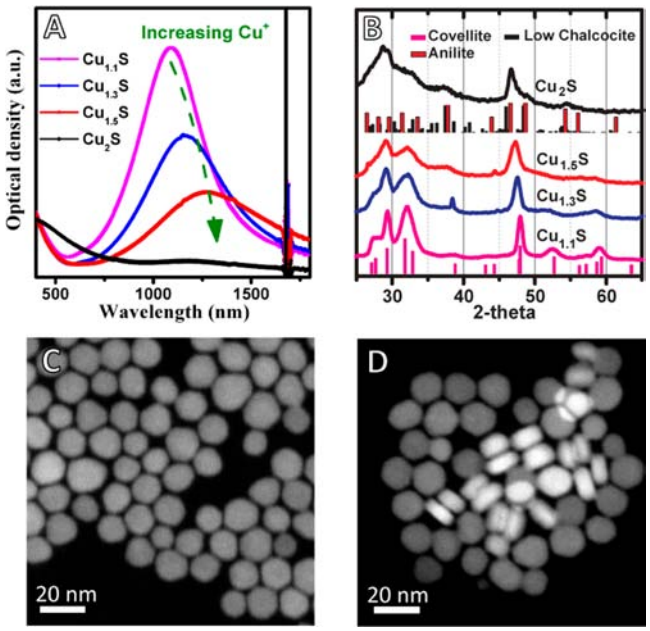

Figure 1. Evolution of the optical extinction spectra (A) and of the XRD patterns collected at room temperature. (B) From the initial $Cu_{1.1}S$ NCs, upon addition of $[Cu(CH_3CN)_4]PF_6$, during which the stoichiometry varied up to Cu_2S. XRD pattern of the $Cu_{1.1}S$ NCs was compatible with covellite (JCPDS Card 79-2321) and instead those of intermediate samples, $Cu_{1.3}S$ and $Cu_{1.5}S$, could be ascribed to a metastable "copper-rich covellite" phase, exhibiting a small shift of the peaks of covellite toward lower angles (see for example the main (110) peak at 48 in 2θ). The XRD pattern of the final sample (Cu_2S) could not be indexed considering just a single phase. This might be again an indication of a metastable structure or of a mixture of copper-rich Cu−S phases, such as low-temperature chalcocite (JCPDS Card 83-1462) and anilite (JCPDS Card 33-0489). (C, D) Representative HAADF-STEM images of the "parent" $Cu_{1.1}S$ covellite sample (C) and of the final Cu_2S sample (D).

stoichiometric covellite phase. Our covellite NCs exhibited a well-defined NIR absorption peak, at around 1090 nm (Figure 1A, cyan spectrum). This peak is ascribable to an in-plane LSPR mode, which dominates the plasmonic response, as found recently by Xie et al.,[15] and is compatible with a free hole density of around 5×10^{21} cm^{-3}, as estimated from the Drude model[11] (see SI for details). This value is of the same order of magnitude as the maximum value found on polycrystalline CuS films (1.7×10^{21} cm^{-3}).[39] Note that here we assumed, for the hole effective mass, a value of $0.8m_e$ (m_e is the electron mass), as extrapolated by Lukashev et al. from calculations on Cu_2S,[40] as we could not find any report on the hole effective mass in covellite from the literature. One however should expect a deviation in the hole effective mass from this value for compounds with Cu:S ratio lower than 2, and therefore at present estimations of free hole densities in these materials should be considered as very rough.

Starting from these NCs, the addition of increasing amounts of Cu(I) complex induced a red shift and decrease in intensity of the NIR absorption band, until a faint absorption was observed at around 1250 nm (see Figure 1A and Figure S2k of the SI for a more complete set of data). Here, the strong feature at 1700 nm is due to the solvent, and indeed spectra recorded on samples dissolved in TCE exhibited only the plasmonic absorption (see Figure S3 of the SI). Upon Cu(I) addition, the NCs were progressively enriched with Cu, as detected by EDS

dx.doi.org/10.1021/ja409754v | J. Am. Chem. Soc. 2013, 135, 17630−17637

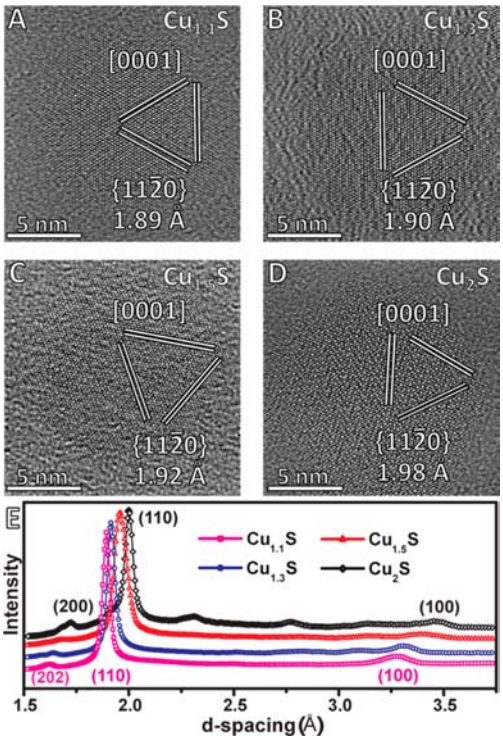

Figure 2. (A–D) HRTEM images of single NCs, with compositions varying from $Cu_{1.1}S$ to Cu_2S showing the $(11\bar{2}0)$ lattice planes with *d*-spacing ranging between 1.89 Å (part A, covellite - JCPDS Card 79-2321) and 1.98 Å (part D, high-temperature chalcocite - JCPDS Card 84-0207). (E) 1D-integrated diffraction patterns obtained from SAED collected on the same samples.

analysis, and the Cu:S ratio in them evolved from 1.1:1 to 2:1 (see Table S1, SI; also note that EDS analysis is generally affected by a 5% error). Please note that, as can be seen by comparing optical data from Figure 1A and Figure S2k of the SI, we were also able to prepare NCs with compositions intermediate between $Cu_{1.5}S$ and Cu_2S. Overall, the present approach is similar to what was reported by us in a previous work, which demonstrated the increase in Cu content of $Cu_{2-x}Se$ NCs by treatment with the same Cu(I) complex as above.[13] Here, as in that work, the red-shift and lowering in intensity in the NIR absorption band is also attributed to the decrease in free carrier density in the NCs due to the increase in Cu stoichiometry.

We also recorded FTIR spectra from films of NCs (both the starting covellite NCs and some representative samples at higher Cu content). Apart from the LSPR absorption discussed above, we could not see any additional plasmon band up to 16 700 nm, neither in the starting covellite nanoplates nor in the other samples obtained from them by reaction with a Cu(I) complex (Figure S4, SI). Our conclusion is that in all these NCs, given the gradual change in the LSPR intensity and spectral position from covellite on, this can be tentatively assigned to an *in-plane* mode, since in covellite the plasmonic response is dominated by the *in-plane* mode. As all the samples that we have prepared in this work have anisotropic crystal structures, it is plausible to contemplate a lower intensity of the out-of-plane LSPR mode to the point that it is not resolved in the spectra, also because it might partially overlap with the in-plane mode. Similarly, Kriegel et al. found a strong damping of the LSPR more along the unique *c* axis of $Cu_{2-x}Te$ nanorods (and arms of tetrapods).[19] Our results are different from the previous report by Hsu et al. on $Cu_{2-x}S$ nanodisks,[12] which apparently showed two extinction bands near 1800 and 3100 nm, attributed, respectively, to out-of-plane and in-plane LSPRs.

These variations in Cu stoichiometry had little influence on the shape of the particles (compare Figures 1C and 1D, corresponding to the initial $Cu_{1.1}S$ NC and the Cu_2S NC, respectively, and Figure S2a–h, SI) and were accompanied only by a small size increase in the diameter (around 5%, going from 13 nm of parent covellite NCs to 13.7 nm of the final Cu_2S NCs, see Figure S2l-n and Table S1 of the SI) and thickness (around 6%, from 5.0 nm of the parent NCs to 5.3 nm of the final Cu_2S NCs, see Figure S2l-n, SI). We also attempted to vary the Cu:S ratio in NCs using the recently reported method of Sines et al.,[41] who were able to convert several metal dichalcogenides to metal chalcogenides by partial extraction of chalcogenides with trioctylphosphine at high temperatures. Starting from the covellite NCs synthesized by us, we could indeed increase their Cu stoichiometry, with a final product consisting of a mixture of phases. However, this came at the expense of severe degradation in the size and shape distribution of the NCs and their aggregation (see Figure S5 of the SI). Therefore, the strategy of reacting the NCs with a Cu(I) complex to increase the Cu content is clearly more appealing if we wish to preserve sizes and shapes of the starting particles.

The NCs, besides the changes in optical properties and in chemical composition by addition of Cu(I) ions, underwent structural changes, as evidenced by XRD (Figure 1B). In particular, the main Bragg reflections of the "parent" $Cu_{1.1}S$ NC sample, indexed as diffraction peaks of covellite, experienced a progressive shift toward lower 2θ angles and weakening in intensity. This is quite clear for the patterns of the samples at intermediate $Cu_{1.3}S$ and $Cu_{1.5}S$ composition, which however still resembled those of the initial covellite NCs, but with a greater amount of copper in the lattice. These patterns are different from those of known copper-rich phases of bulk covellite, often referred to as *"Blaubleibender covellite"*.[42] The latter can be considered as superstructures of the hexagonal covellite subcell. The XRD pattern of *Blaubleibender covellite* is very similar to that of stoichiometric covellite, except for the intensity of the (108) and (116) reflections (at 52 and 58 in 2θ degrees, respectively), which are much weaker than in normal covellite.[42] Apart from that, all peak positions remain the same as those of covellite. In our case instead the peak positions shifted too, as we are intercalating a large number of Cu species in the initial covellite lattice. Therefore, our $Cu_{1.3}S$ and $Cu_{1.5}S$ NCs can be considered as having a metastable structure, since there are no known stable phases in the Cu–S system in that range of composition. It is actually not uncommon to step into metastable structures when studying chemical transformations in nanostructures[43] or, more in general, when following the so-called "soft chemistry" approaches to materials synthesis.[44]

The complete series of NCs recovered after reaction with different volumes moles of the Cu(I) complex is reported in the SI (Figure S2i–j). The pattern of the samples with a Cu:S ratio higher than 1.5:1, as well as the final Cu_2S sample, could not be indexed considering just a single phase. This might be again an indication of a metastable structure, or of a mixture of the orthorhombic $Cu_{2-x}S$ anilite (JCPDS Card 33-0489) and monoclinic low chalcocite (Cu_2S) (JCPDS Card 83-1462), both low-temperature phases, and even the presence of additional monoclinic $Cu_{2-x}S$ djurleite (JCPDS Card 83-1463) could not be ruled out (see SI). In general, heating of

dx.doi.org/10.1021/ja409754v | J. Am. Chem. Soc. 2013, 135, 17630–17637

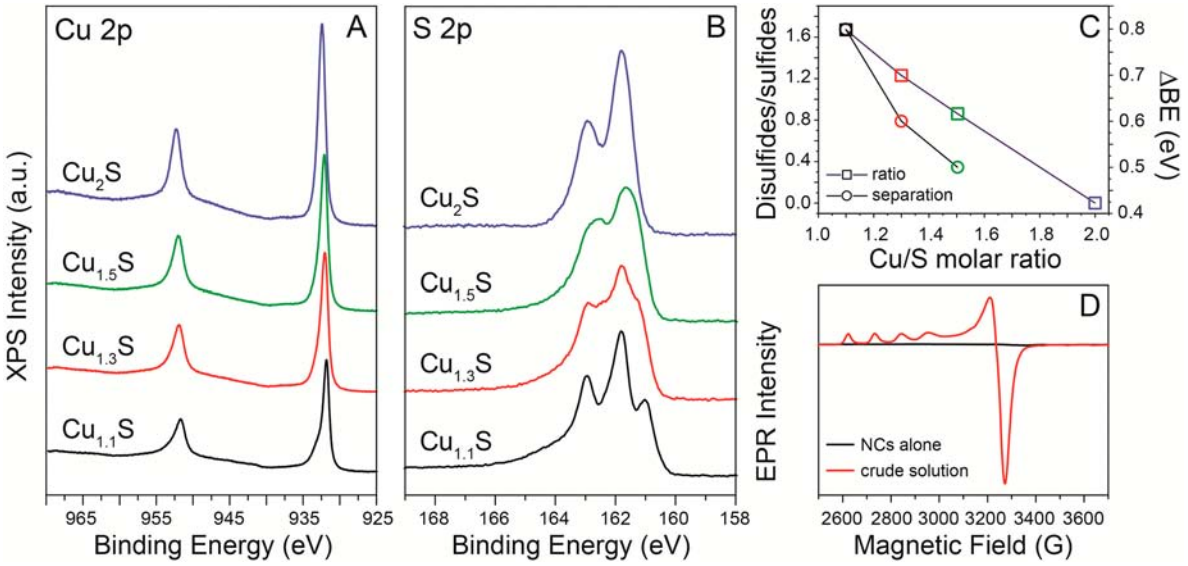

Figure 3. High-resolution XPS characterization of starting $Cu_{1.1}S$ NCs and of three samples obtained after addition of increasing amounts of the Cu(I) complex. (A) Cu 2p region. (B) S 2p region. (C) Ratio and energy separation of the disulfide and sulfide components as functions of the Cu/S ratio in the four analyzed samples, as obtained by spectra decomposition (see SI for details). As the Cu content in the NCs increased, the relative amount of disulfides decreased, going to zero in the Cu_2S NCs. At the same time, the energy separation between the sulfide and disulfide components decreased. (D) EPR signals collected on a crude solution (red line) of $Cu_{1+\gamma}S$ NCs (obtained by adding 9 mL of the Cu(I) complex solution to 5 mL of the parent covellite NC solution) and on the cleaned NCs alone (black line). While the spectrum of the crude solution clearly indicates the presence of paramagnetic species (i.e., Cu(II) formed during the reaction, see SI for details), no EPR signal was observed in the NCs, confirming that the oxidation state of Cu in the NCs is +1.

the samples caused changes in their XRD patterns. For example, upon heating the final Cu_2S sample at 150 °C under N_2, its pattern evolved in a way that it could be rather indexed to the high chalcocite phase (see Figure S12, SI, for details).

HRTEM characterizations and lattice parameter analysis of selected NCs from each sample (Figure 2A–D) indicated that the angular relationships of crystal directions maintained a hexagonal symmetry, while *d*-spacings varied gradually from $Cu_{1.1}S$ to Cu_2S. This was best clarified by converting the conventional 2D electron diffraction patterns of selected area electron diffraction (SAED) from the various samples to linear 1D diffractograms,[45] as reported in Figure 2E. Here, the variation of the interplanar distances caused by the enrichment with copper can be immediately observed as a shift toward higher *d*-spacings, expressed in Å. It is actually possible to show that the transition from covellite to various other Cu–S phases (low chalcocite, anilite, high chalcocite, etc.), upon addition of copper, entails minor distortions of the underlying anionic sulfur sublattices, apart from the initial breaking of the S–S bonds present in the sole covellite phase. This is discussed in detail in the SI. It is also interesting to note that neither low chalcocite nor anilite phases were seen under HRTEM analysis of the Cu_2S sample (Figure 2D). Indeed, it is known that stable low-temperature $Cu_{2-x}S$ phases such as digenite ($Cu_{1.8}S$) and djurleite ($Cu_{1.96}S$) undergo phase transition to structures with higher symmetry in the presence of high temperatures[46] or under electron beam exposure.[47] It is likely therefore that the Cu_2S NCs in such lower temperature phases quickly evolved to the high chalcocite phase when analyzed by us in the electron microscope.

It is noteworthy to correlate the structural, compositional, and optical variations, when increasing the Cu content in the NCs, to changes in the underlying electronic structure, especially for what concerns the valency of the cations and anions in the lattice. According to a simplified approach, in copper chalcogenides ($Cu_{2-x}E$, with E = S, Se, Te) the top of the valence band has a strong contribution from the chalcogenide p orbitals, while the bottom of the conduction band is mainly built from Cu 4s and 4p orbitals (see for example ref 48 for the $Cu_{2-x}Se$ case). To a first approximation, each Cu atom contributes with one 4s electron and each chalcogen atom with six p electrons to bonding. In a fully stoichiometric Cu_2E compound, the valence band is thus completely filled. Whenever Cu vacancies are created, this leaves holes in the top of the valence band, which means that the valency of the chalcogenide is mainly affected, while the valency of Cu should remain close to +1. Covellite CuS (as well as CuSe and CuTe) is actually a peculiar case, as reflected by the unique structure of covellite: this can be described by a repetitive unit composed of a layer of triangular CuS_3 units, sandwiched between two layers made of CuS_4 tetrahedra (see Figure S9 in the SI). Each triple layer is then linked to a top and bottom triple layer with disulfide bonds.[49] In covellite, the valency of copper is still debated. Some studies have found monovalent copper, suggesting a $(Cu^{1+})_3(S_2^{2-})(S^{1-})$[50] or a $(Cu^{1+})_3(S_2^{-})(S^{2-})$[51] valency formalism for CuS. According to both studies then the valency of sulfur is equal to −1 (−1 for all S ions in ref 50 and −1 as an average value in ref 51). Other studies instead have indicated the presence of both Cu(I) and Cu(II) (proposing a $(Cu^{2+})(S_2^{2-})(Cu^{1+})_2(S^{2-})$[52,53] formulation), and recent experiments and calculations have put the valency of Cu between 1 and 1.5 (1.33 for CuS from calculations).[54]

With the aim of elucidating the valency of Cu and S in the various NC samples of this work, we carried out XPS analysis and corroborated these data with EPR and SQUID measurements, which are sensitive to paramagnetic (Cu^{2+}) species in the samples. The Cu 2p spectrum of the initial covellite NCs (Figure 3A, black curve), together with the results of SQUID

dx.doi.org/10.1021/ja409754v | J. Am. Chem. Soc. 2013, 135, 17630–17637

measurements at 300 K (Figure S13, SI), indicated that the oxidation state of Cu was basically +1 (the NCs exhibited indeed a diamagnetic behavior).[55] The XPS Cu peaks of these NCs were characterized by an asymmetric tail, already known for covellite[56] and typical of metals, due to kinetic energy losses in the interaction of photoelectrons with free charge carriers.[57] The asymmetric tail was gradually reduced in the samples that were progressively richer in Cu (Figure 3A). In analogy with the case of metals,[57] this could be rationalized as due to a decrease in the density of free holes. Also in these samples no Cu(II) species were present, indicating that the Cu valency remained close to 1 in all the NCs after addition of the Cu(I) complex. Here again, the absence of Cu(II) species in the NCs was corroborated by EPR spectra of extensively washed NC samples, from which no paramagnetic signal could be detected (Figure 3D).

Several interesting changes were observed instead in the S 2p region, during the evolution from $Cu_{1.1}S$ to Cu_2S. In the starting $Cu_{1.1}S$ NCs, the S 2p band (Figure 3B, black curve) was characterized by the "three peaks" profile typical for covellite.[58] Deconvolution in subcomponents (Figure S6 of SI) revealed the presence of two main doublets, which are characteristic of sulfide (at BE of 161.0 ± 0.2 eV) and disulfide (161.8 ± 0.2 eV BE) moieties in covellite. The ratio of the areas under the curves of the disulfide and the sulfide components was 1.7:1, close to 2:1, as expected for pure covellite. During the evolution from $Cu_{1.1}S$ to Cu_2S, the intensity ratio between the disulfide and the sulfide components gradually decreased (until no disulfides were present in the Cu_2S NCs) together with the energy separation between the two components (see Figure 3B,C). In particular, the position of the sulfide peak evolved from 161 to ∼161.8 eV, reflecting the increase in average Cu−S bond length, which is shorter in covellite than in chalcocite[59] (see also Figure S6 in the SI).

Overall, our analysis supports a constant valency of Cu, around 1, in all the samples, while the average −1 valence of S of covellite gradually evolved to −2 when increasing the Cu content in the NCs. This is corroborated by previous XPS studies on bulk copper sulfides.[60−62] The reaction of the starting covellite NCs with the Cu(I) complex is therefore a reduction which occurs prevalently on the sulfur anion sublattice. By considering together the data from XPS, compositional, and structural analysis, we can make interesting comparisons between the enrichment in Cu of the initial covellite NCs and the intercalation of metal species in transition metal dichalcogenides[63] (TMDCs, for example via an electrochemical process[64]). In both cases, the insertion of metal ions leads to minor structural changes (for covellite NCs this is valid only for the first stages of Cu insertion), as we are mainly breaking dichalcogenide bonds and intercalating metals. In a TMDC, with general formula MX_2, the valency of the M cation is +4 and that of the chalcogen (X) is −2, and the layers are held together by weak van der Waals bonds between the chalcogenide anions terminating each layer.[63] The addition of metal ions in between the layers of a TMDC must be matched by an inflow of electrons to the TMDC, which end up occupying the partially filled d bands of the transition metal M^{4+} cation framework. In the case of direct intercalation of neutral metal atoms,[65] an electron transfer occurs from such metal atoms to the d orbitals of the M^{4+} cation framework. Therefore, mainly the valency of the cation framework is affected. In covellite instead the layers are held together by S−S *covalent* bonds, and when such bonds are broken following the incorporation of Cu(I) species, mainly the valency of sulfur anions is affected.

The reduction on the anion sublattice in the covellite NCs discussed here, complemented by an increase in Cu content in the NCs, must be paralleled by an oxidation process in solution. We proved, by EPR spectroscopy, that the reaction of the NCs with the Cu(I) complex lead to the formation of Cu(II) species in the solution (see Figure 3D). Furthermore, comparison of data from EPR with elemental analysis of the NCs (Figure S7 and Table S3 of SI), before and after their reaction with the Cu(I) complex, indicated that the increase in Cu content in the NCs was associated with the formation of a comparable amount of Cu(II) species in solution (see Figure 4).

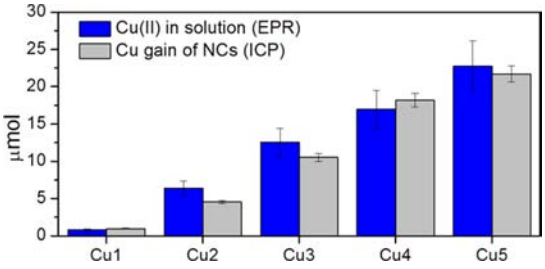

Figure 4. Cu(II) amount (in μmol) measured by EPR and Cu amount gained by the NCs measured by elemental analysis (via ICP) on properly cleaned samples, for a series of experiments in which increasing amounts of Cu(I) complex were added to a starting sample of $Cu_{1.1}S$ NCs. Error bars display the standard deviation. Since the resulting NCs exhibited no paramagnetic signal (see Figure 3D), EPR analyses could be carried out directly on the crude solutions (i.e., containing the NCs, the residual Cu(I) complex, and any Cu(II) species formed, see SI for additional details).

There could be several mechanisms by which the overall redox reaction described in this work (reduction of the NCs, by increase of their Cu content, paralleled by the formation of Cu(II) species in solution) can take place. According to a plausible mechanism, a fraction of Cu^+ ions (γ moles) from the solution phase enters the NC lattice, matched by a transfer of γ moles of electrons from the solution, i.e.

$$Cu_{1.1}S + \gamma Cu(I) + \gamma e^- \rightarrow Cu_{1.1+\gamma}S$$

The same reaction was actually hypothesized by Shah and Khalafalla as one of the steps involved in the roasting of CuS pellets under air to CuO, which formed $Cu_{1.8}S$ as an intermediate compound.[66] Electrons in our case are supplied by an equimolar amount of Cu(I) species remaining in solution and being oxidized to Cu(II). Other mechanisms are plausible too, and they differ from each other only for what concerns the initial oxidation state of the Cu species entering the NCs, which however becomes +1 once they are incorporated in the NCs (as shown by XPS). These various plausible mechanisms are briefly discussed in the SI. It turns out that, regardless of the detailed mechanism, the overall reaction is always the following one (see SI)

$$Cu_{1.1}S + 2\gamma Cu(I) \rightarrow Cu_{1.1+\gamma}S + \gamma Cu(II)$$

The oxidation of a fraction of Cu(I) species to Cu(II), in parallel with the enrichment in the Cu content in the NCs, is also supported by the solvent-dependent kinetics of the reaction: when using methanol as a solvent to dissolve $[Cu(CH_3CN)_4]PF_6$, the reduction of the NCs, as followed by

dx.doi.org/10.1021/ja409754v | J. Am. Chem. Soc. 2013, 135, 17630−17637

recording optical extinction spectra, could be observed already a few seconds after addition of the Cu(I) complex (Figure S8a, SI). Methanol is indeed a hard Lewis base which should stabilize the hard Lewis acid Cu^{2+} and therefore promote the oxidation of Cu(I) to Cu(II). When using instead solvents like acetone or acetonitrile (both good solvents for Cu-$(CH_3CN)_4PF_6$) the reaction was greatly slowed down (Figure S8b,c, SI). This is understandable because both acetone and acetonitrile are soft Lewis bases (relative to methanol), which instead tend to stabilize the soft Cu^+ acid. Also, it is worth recalling here that other groups have used different chemicals to quench the plasmon resonance in Cu_2E (E = S, Se, Te) NCs. Kriegel et al. for example[14] used diisobutylaluminium hydride (DIBAH) instead of Cu^+ ions as the reducing agent. However, since no extra Cu species were introduced, it remains unclear how the Cu stoichiometry in that case was re-established from $Cu_{2-x}E$ to Cu_2E.

CONCLUSIONS

Platelet-shaped covellite NCs could be synthesized by a heat-up procedure. The Cu:S ratio in these NCs could then be gradually increased from 1.1:1 to 2:1, by a versatile postsynthesis reaction of the NCs with $Cu(CH_3CN)_4PF_6$ in methanol/toluene while retaining their overall size and morphology. This was accompanied by structural and optical changes in the particles. Most notably, the NIR LSPR band red-shifted, and its intensity decreased until the band vanished, with increasing incorporation of Cu in the lattice. The overall process could be described as a reduction of the NCs, with the framework of S anions evolving from a −1 valency to −2 in the final Cu_2S NCs, while the valency in the framework of Cu cations stayed close to +1. The reduction of the anion framework was matched by the oxidation of a fraction of the Cu(I) species that had remained in solution and were oxidized to Cu(II). In principle, this approach of using Cu(I) species as sacrificial electron donors might be exploited to insert other chemical species, in addition to Cu or preferentially to Cu, into an initial "host lattice" of CuE (E = S, Se, Te) NCs and might pave the way to a new class of interesting chemical transformations in colloidal nanostructures.

ASSOCIATED CONTENT

Supporting Information

Additional STEM-HAADF and SAED data on as-synthesized covellite NCs; experiments related to the reaction of as-synthesized NCs with trioctylphosphine; additional XPS, EPR, optical, and ICP data; discussion on the possible mechanisms involved in the reaction of covellite NCs with Cu(I) species; discussion on the crystal structure evolution from covellite to chalcocite. This material is available free of charge via the Internet at http://pubs.acs.org.

AUTHOR INFORMATION

Corresponding Author

liberato.manna@iit.it

Notes

The authors declare no competing financial interest.

ACKNOWLEDGMENTS

The research leading to these results has received funding from the European Union's Seventh Framework Programme FP7/2007-2013 under grant agreement n. 240111 (ERC Grant NANO-ARCH). We thank Mauro Povia for help with the XRD experiments and Maria Fittipaldi for the many stimulating discussions.

REFERENCES

(1) Liu, G.; Schulmeyer, T.; Brötz, J.; Klein, A.; Jaegermann, W. *Thin Solid Films* **2003**, *431−432*, 477−482.
(2) Wu, Y.; Wadia, C.; Ma, W.; Sadtler, B.; Alivisatos, A. P. *Nano Lett.* **2008**, *8*, 2551−2555.
(3) Lee, H.; Yoon, S. W.; Kim, E. J.; Park, J. *Nano Lett.* **2007**, *7*, 778−784.
(4) Basu, M.; Sinha, A. K.; Pradhan, M.; Sarkar, S.; Negishi, Y.; Govind; Pal, T. *Environ. Sci. Technol.* **2010**, *44*, 6313−6318.
(5) Lai, C. H.; Huang, K. W.; Cheng, J. H.; Lee, C. Y.; Hwang, B. J.; Chen, L. J. *J. Mater. Chem.* **2010**, *20*, 6638−6645.
(6) Šetkus, A.; Galdikas, A.; Mironas, A.; Šimkiene, I.; Ancutiene, I.; Janickis, V.; Kaciulis, S.; Mattogno, G.; Ingo, G. M. *Thin Solid Films* **2001**, *391*, 275−281.
(7) Riha, S. C.; Johnson, D. C.; Prieto, A. L. *J. Am. Chem. Soc.* **2011**, *133*, 1383−1390.
(8) Kreibig, U.; Vollmer, M. *Optical Properties of Metal Clusters*; Springer-Verlag: Berlin, 1995.
(9) Raether, H. *Surface Plasmon on Smooth and Rough Surfaces and on Gratings*; Springer: Berlin, 1988.
(10) Zhao, Y. X.; Pan, H. C.; Lou, Y. B.; Qiu, X. F.; Zhu, J. J.; Burda, C. *J. Am. Chem. Soc.* **2009**, *131*, 4253−4261.
(11) Luther, J. M.; Jain, P. K.; Ewers, T.; Alivisatos, A. P. *Nat. Mater.* **2011**, *10*, 361−366.
(12) Hsu, S. W.; On, K.; Tao, A. R. *J. Am. Chem. Soc.* **2011**, *133*, 19072−19075.
(13) Dorfs, D.; Härtling, T.; Miszta, K.; Bigall, N. C.; Kim, M. R.; Genovese, A.; Falqui, A.; Povia, M.; Manna, L. *J. Am. Chem. Soc.* **2011**, *133*, 11175−11180.
(14) Kriegel, I.; Jiang, C.; Rodríguez-Fernández, J.; Schaller, R. D.; Talapin, D. V.; Como, E. d.; Feldmann, J. *J. Am. Chem. Soc.* **2012**, *134*, 1583−1590.
(15) Xie, Y.; Carbone, L.; Nobile, C.; Grillo, V.; D'Agostino, S.; Della Sala, F.; Giannini, C.; Altamura, D.; Oelsner, C.; Kryschi, C. *ACS Nano* **2013**, *7*, 7352−7369.
(16) Zhao, Y. X.; Burda, C. *Energy Environ. Sci.* **2012**, *5*, 5564−5576.
(17) Routzahn, A. L.; White, S. L.; Fong, L. K.; Jain, P. K. *Isr. J. Chem.* **2012**, *52*, 983−991.
(18) Hessel, C. M.; Pattani, V. P.; Rasch, M.; Panthani, M. G.; Koo, B.; Tunnell, J. W.; Korgel, B. A. *Nano Lett.* **2011**, *11*, 2560−2566.
(19) Kriegel, I.; Rodríguez-Fernández, J.; Wisnet, A.; Zhang, H.; Waurisch, C.; Eychmüller, A.; Dubavik, A.; Govorov, A. O.; Feldmann, J. *ACS Nano* **2013**, *7*, 4367−4377.
(20) Kanehara, M.; Koike, H.; Yoshinaga, T.; Teranishi, T. *J. Am. Chem. Soc.* **2009**, *131*, 17736−17737.
(21) Franzen, S. *J. Phys. Chem. C* **2008**, *112*, 6027−6032.
(22) Garcia, G.; Buonsanti, R.; Runnerstrom, E. L.; Mendelsberg, R. J.; Llordes, A.; Anders, A.; Richardson, T. J.; Milliron, D. J. *Nano Lett.* **2011**, *11*, 4415−4420.
(23) Buonsanti, R.; Llordes, A.; Aloni, S.; Helms, B. A.; Milliron, D. J. *Nano Lett.* **2011**, *11*, 4706−4710.
(24) Huang, Q. Q.; Hu, S.; Zhuang, J.; Wang, X. *Chem.—Eur. J.* **2012**, *18*, 15283−15287.
(25) Manthiram, K.; Alivisatos, A. P. *J. Am. Chem. Soc.* **2012**, *134*, 3995−3998.
(26) Manna, G.; Bose, R.; Pradhan, N. *Angew. Chem., Int. Ed.* **2013**, *52*, 6762−6766.
(27) Polking, M. J.; Jain, P. K.; Bekenstein, Y.; Banin, U.; Millo, O.; Ramesh, R.; Alivisatos, A. P. *Phys. Rev. Lett.* **2013**, *111*, 127601.
(28) Han, W.; Yi, L.; Zhao, N.; Tang, A.; Gao, M.; Tang, Z. *J. Am. Chem. Soc.* **2008**, *130*, 13152−13161.
(29) Larsen, T. H.; Sigman, M.; Ghezelbash, A.; Doty, R. C.; Korgel, B. A. *J. Am. Chem. Soc.* **2003**, *125*, 5638−5639.

(30) Chu, L.; Zhou, B.; Mu, H.; Sun, Y.; Xu, P. *J. Cryst. Growth* **2008**, *310*, 5437−5440.
(31) Sadtler, B.; Demchenko, D. O.; Zheng, H.; Hughes, S. M.; Merkle, M. G.; Dahmen, U.; Wang, L. W.; Alivisatos, A. P. *J. Am. Chem. Soc.* **2009**, *131*, 5285−5293.
(32) Singh, K. V.; Martinez-Morales, A. A.; Andavan, G. T. S.; Bozhilov, K. N.; Ozkan, M. *Chem. Mater.* **2007**, *19*, 2446−2454.
(33) Kruszynska, M.; Borchert, H.; Bachmatiuk, A.; Rümmeli, M. H.; Büchner, B.; Parisi, J.; Kolny-Olesiak, J. *ACS Nano* **2012**, *6*, 5889−5896.
(34) Kumar, P.; Nagarajan, R. *Inorg. Chem.* **2011**, *50*, 9204−9206.
(35) Kundu, M.; Hasegawa, T.; Terabe, K.; Yamamoto, K.; Aono, M. *Sci. Technol. Adv. Mater.* **2008**, *9*, 035011.
(36) Son, D. H.; Hughes, S. M.; Yin, Y.; Alivisatos, A. P. *Science* **2004**, *306*, 1009−1012.
(37) Jain, P. K.; Beberwyck, B. J.; Fong, L.-K.; Polking, M. J.; Alivisatos, A. P. *Angew. Chem., Int. Ed.* **2012**, *51*, 2387−2390.
(38) Rivest, J. B.; Jain, P. K. *Chem. Soc. Rev.* **2013**, *42*, 89−96.
(39) Adelifard, M.; Eshghi, H.; Mohagheghi, M. M. B. *Appl. Surf. Sci.* **2012**, *258*, 5733−5738.
(40) Lukashev, P.; Lambrecht, W. R. L.; Kotani, T.; van Schilfgaarde, M. *Phys. Rev. B* **2007**, *76*, 195202.
(41) Sines, I. T.; Schaak, R. E. *J. Am. Chem. Soc.* **2010**, *133*, 1294−1297.
(42) Putnis, A.; Grace, J.; Cameron, W. E. *Contrib. Mineral. Petrol.* **1977**, *60*, 209−217.
(43) Li, H.; Zanella, M.; Genovese, A.; Povia, M.; Falqui, A.; Giannini, C.; Manna, L. *Nano Lett.* **2011**, *11*, 4964−4970.
(44) Gopalakrishnan, J. *Chem. Mater.* **1995**, *7*, 1265−1275.
(45) Gammer, C.; Mangler, C.; Rentenberger, C.; Karnthaler, H. P. *Scr. Mater.* **2010**, *63*, 312−315.
(46) Okamoto, K.; Kawai, S. *Jpn. J. Appl. Phys.* **1973**, *12*, 1130−1138.
(47) Putnis, A. *Am. Mineral.* **1977**, *62*, 107−114.
(48) Garba, E. J. D.; Jacobs, R. L. *Phys. B+C* **1986**, *138*, 253−260.
(49) Casaca, A.; Lopes, E. B.; Gonçalves, A. P.; Almeida, M. *J. Phys.: Condens. Matter* **2012**, *24*, 015701.
(50) Fjellvåg, H.; Grønvold, F.; Stølen, S.; Andresen, A. F.; Müller-Käfer, R.; Simon, A. *Z. Kristallogr.* **1988**, *184*, 111−121.
(51) Liang, W.; Whangbo, M. H. *Solid State Commun.* **1993**, *85*, 405−408.
(52) Grioni, M.; Goedkoop, J. B.; Schoorl, R.; de Groot, F. M. F.; Fuggle, J. C.; Schäfers, F.; Koch, E. E.; Rossi, G.; Esteva, J. M.; Karnatak, R. C. *Phys. Rev. B* **1989**, *39*, 1541−1545.
(53) Kumar, P.; Nagarajan, R.; Sarangi, R. *J. Mater. Chem. C* **2013**, *1*, 2448−2454.
(54) Mazin, I. I. *Phys. Rev. B* **2012**, *85*, 115133.
(55) Biesinger, M. C.; Lau, L. W. M.; Gerson, A. R.; Smart, R. S. C. *Appl. Surf. Sci.* **2010**, *257*, 887−898.
(56) Goh, S. W.; Buckley, A. N.; Lamb, R. N.; Rosenberg, R. A.; Moran, D. *Geochim. Cosmochim. Acta* **2006**, *70*, 2210−2228.
(57) Briggs, D.; Seah, P. M. *Practical Surface Analysis: Auger and X-ray photoelectron spectroscopy*; Wiley: New York, 1990.
(58) Laajalehto, K.; Kartio, I.; Kaurila, T.; Laiho, T.; Suoninen, E. *Proc. 6th Eur. Conf. Appl. Surf. Interface Anal. ECASIA '95*; Reihl, B., Briggs, D., Eds.; Wiley: New York, 1996.
(59) Evans, H. T. J. *Am. Mineral.* **1981**, *66*, 807−818.
(60) Folmer, J. C. W.; Jellinek, F. *J. Less Common Met.* **1980**, *76*, 153−162.
(61) Nakai, I.; Sugitani, Y.; Nagashima, K.; Niwa, Y. *J. Inorg. Nucl. Chem* **1978**, *40*, 789−791.
(62) Perry, D.; Taylor, J. A. *J. Mater. Sci. Lett.* **1986**, *5*, 384−386.
(63) Chhowalla, M.; Shin, H. S.; Eda, G.; Li, L.-J.; Loh, K. P.; Zhang, H. *Nat. Chem.* **2013**, *5*, 263−275.
(64) Julien, C. M. *Mater. Sci. Eng. R* **2003**, *40*, 47−102.
(65) Lévy, F. A. *Intercalated Layered Materials*; D. Reidel Publishing Company: Dordrecht, Holland, 1979; Vol. *6*.
(66) Shah, I. D.; Khalafal, Se. *Metall. Trans.* **1971**, *2*, 2637−2643.